Direct calculation of the attempt frequency of magnetic structures using the finite element method

G. Fiedler, J. Fidler, J. Lee, T. Schrefl, R. L. Stamps, H. B. Braun, and D. Suess

Citation: Journal of Applied Physics **111**, 093917 (2012); doi: 10.1063/1.4712033
View online: http://dx.doi.org/10.1063/1.4712033
View Table of Contents: http://scitation.aip.org/content/aip/journal/jap/111/9?ver=pdfcov
Published by the AIP Publishing

Direct calculation of the attempt frequency of magnetic structures using the finite element method

G. Fiedler,[1] J. Fidler,[1] J. Lee,[1] T. Schrefl,[2] R. L. Stamps,[3] H. B. Braun,[4] and D. Suess[1,a)]
[1]*Institute of Solid State Physics, Vienna University of Technology, Vienna 1040, Austria*
[2]*St. Poelten University of Applied Sciences, St. Poelten 3130, Austria*
[3]*School of Physics, M013, University of Western Australia, 35 Stirling Hwy, Crawley Western Australia 6009, Australia*
[4]*UCD School of Physics, University College Dublin, Belfield, Dublin 4, Ireland*

(Received 11 August 2011; accepted 7 April 2012; published online 10 May 2012)

A numerical implementation of the transition state theory is presented which can be used to calculate the attempt frequency f_0 of arbitrary shaped magnetic nanostructures. The micromagnetic equations are discretized using the finite element method. The climbing image nudged elastic band method is used to calculate the saddle point configuration, which is required for the calculation of f_0. Excellent agreement of the implemented numerical model and analytical solutions is obtained for single domain particles. The developed method is applied to compare f_0 for single phase and graded media grains of advanced recording media. f_0 is predicted to be comparable if the maximum anisotropy is the same in these two media types. © *2012 American Institute of Physics*. [http://dx.doi.org/10.1063/1.4712033]

I. INTRODUCTION

A detailed knowledge of the thermal stability is of utmost importance for magnetic nanostructures for various applications ranging from hard disc media, magnetoresistive random-access memory (MRAM) devices to permanent magnets. A well established tool which originated in chemical rate theory for determining the thermal stability relies on the transition state theory (TST). In the TST, the thermal stability of a minimum energy state M_1 is determined by the application of the Arrhenius-Neel law, $\tau = \frac{1}{f_0} e^{\frac{\Delta E}{k_B T}}$, where the energy barrier ΔE separates the minimum energy state M_1 and the saddle point configuration S_1. The energy denotes the total energy which is the sum of the internal energy plus the Zeeman energy. The internal energy accounts for the anisotropy energy, the exchange energy, and the magnetostatic energy. At zero temperature, the sum of the internal energy plus the Zeeman energy equals the Gibbs free energy. The thermal stability, which requires the calculation of the energy barrier and the attempt frequency, was first calculated for single domain particles in the intermediate to high damping limit (IHD) for an external field applied exactly parallel to the easy axis.[3] For systems where the symmetry is broken either by an oblique external field or by an additional anisotropy, various works are published giving analytical formulas for the attempt frequency for different damping limits. For the IHD limit, formulas for the thermal stability can be found in Refs. 2, 4, 5, and 19. For the limit of very low damping, a formula for the thermal stability was derived by Smith and De Rozario.[19] In order to extend the calculation of the damping limit to all values of the damping constant, Coffey *et al.*[6] and Déjardin *et al.*[7] have shown that the Mel'nikov-Meshkov formalism can be applied to magnetic systems. Analytical formulas for the intermediate damping regime are given by Garanin *et al.*[9]

All the previous mentioned works were restricted to reversal via homogeneous rotation. Inhomogenous states were treated by Braun who calculated the thermally activated reversal in elongated particles.[1] Besides analytical formulas for the attempt frequency, he found that the thermal stability depends on the domain wall energy in these elongated particles.

The approach of Braun was extended to soft/hard bilayers, where the saddle point configuration can be described by a domain wall at the soft/hard interface by Loxley and Stamps.[16]

All mentioned previous works dealing with the calculation of the attempt frequency are limited to one or two degrees of freedom. Within the paper for the first time, these restrictions are overcome by using a flexible numerical approach for calculating the attempt frequency. The method uses the hybrid finite element/boundary element method together with the transition state theory, which leads to a general and flexible tool to treat arbitrary shaped magnetic elements with large degrees of freedom. Complicated microstructures such as hard/soft composite magnets can be treated for the first time. The results are for utmost importance for the calculation of the thermal stability of realistic and state of the art magnetic structures. In addition of the calculation of the thermal stability, a detailed knowledge of the attempt frequency is also required if the coercive field of magnets at finite temperature is calculated. Hence, the work has impact on various applications ranging from permanent magnets, magnetic recording, to magnetic logic devices.

The paper is structured as follows. In Sec. II, details of the implementation of the transition state theory in the finite element package finite element micromagnetics (FEMME) (Ref. 23) are given. The implementation method is compared to analytical solutions in Sec. III. An improved method for the calculation of f_0 is presented in Sec. IV. Summary and discussion are given in Sec. V.

a)Author to whom correspondence should be addressed. Electronic mail: suess@magnet.atp.tuwien.ac.at.

II. NUMERICAL CALCULATION OF THE ATTEMPT FREQUENCY

The numerical implementation is based on Kramers transition state theory,[13] which Langer transposed and expanded to multidimensional systems in 1967.[14] As an assumption for the transition state theory one has to assume that the energy barrier separating the stable states is much higher than the thermal energy K_BT.Hence, the transition rate theory is restricted to low temperature. An other assumption is that the basic transition state theory is limited to the intermediate high damping limit. Hence, only magnetic systems where the precessional motion of the system can be neglected can be treated. One consequence of the intermediate to high damping limit is that the obtained attempt frequencies do not depend on the temperature, which is generally not correct. Besides these limitations, the transition state theory is successfully applied in various applications ranging from the calculation of enthalpy of chemical reactions to nucleation processes in condensed matter physics.

According to Langers approach, the attempt frequency determines the probability current for the configuration distribution on the energy surface around the saddle point.

The following steps are required in order to calculate the attempt frequency by the means of the transition state theory:

1. The configuration of the system at the minimum and at the saddle point given as the values of all degrees of freedom.
2. The value and curvature of the total energy surface at the minimum and at the saddle point with respect to appropriate canonical variables.
3. The systems' equation of motion in canonical variables along the energy surface to describe the dynamics around the saddle point.

Knowledge of the above properties allows one to calculate the attempt frequency. This can be written as

$$f_0 = \frac{\lambda_+}{2\pi}\Omega_0. \tag{1}$$

Here, λ_+ denotes for the dynamical prefactor taking into account for the equation of motion of the system and Ω_0 is the ratio of the well and saddle angular frequencies.

A. Dynamical factor λ_+ from the Landau-Lifshitz-Gilbert equation

The dynamical factor λ_+ is obtained by solving the noiseless linearized equation of motion. In micromagnetics, the equation of motion can be written in the form of the Landau-Lifshitz-Gilbert equation as,

$$\frac{\partial}{\partial t}\vec{J} = -\frac{\gamma}{1+\alpha^2}\vec{J}\times\overrightarrow{H_{eff}} - \frac{\alpha}{1+\alpha^2}\frac{\gamma}{J_S}\vec{J}\times(\vec{J}\times\overrightarrow{H_{eff}}), \tag{2}$$

where the magnetic polarization $\vec{J}$ and the effective $\overrightarrow{H_{eff}}$ field are continuous functions of space. In the following, we discretize the continuous equation of motion using the finite element method using the box scheme.[11,23] We can write for the effective field on the node point i,

$$H_{eff,i} \approx -\frac{1}{V_i}\left(\frac{\partial E}{\partial J_i}\right) \tag{3}$$

with V_i being the corresponding volume of spin i and E being the total energy. The structure of the Landau-Lifshitz-Gilbert equation leads to a constant length of the magnetic polarization $|\vec{J}| = J_s$. As a consequence, the number of independent equations is $2N$, where N is the number of spins. In order to apply the theory developed by Langer, the system has to be expressed with its canonical variables.[14] For a system with N-spins, the canonical variables on node point i are given by,[10,17]

$$\begin{aligned} p_i &= V_i J_s \cos(\theta_i) \\ q_i &= \phi_i, \end{aligned} \tag{4}$$

where the polar angle angle ϕ_i and azimuthal angle θ_i are defined as,

$$\overrightarrow{J_i} = J_s(\sin\theta_i\cos\phi_i, \sin\theta_i\sin\phi_i, \cos\theta_i). \tag{5}$$

The definition of the canonical variables p_i and q_i is convenient since the determinate of the Jacobian matrix

$$det\left(\frac{\partial(J_{i,x}, J_{i,y}, J_{i,z})}{\partial(p_i, q_i, J_s)}\right) = const \tag{6}$$

is constant and does not depend on the angle ϕ_i or θ_i. This is in contrast to the formulation where instead of p_i and q_i, the spherical coordinates ϕ_i and θ_i are used. In this case, the determinate of the Jacobian contains a term $\sin(\theta_i)$ and the transition state theory cannot used in the simple form as given by Eq. (1) but rather would require to include the non constant Jacobian.

The Landau-Lifshitz-Gilbert equation for spin i in canonical variables reads,

$$\begin{aligned} \begin{pmatrix} \frac{\partial p_i}{\partial t} \\ \frac{\partial q_i}{\partial t} \end{pmatrix} &= -\frac{\gamma}{J_s V_i(1+\alpha^2)}\frac{1}{\sin\theta_i} \\ &\times \begin{pmatrix} -J_s V_i \alpha \sin^2\theta_i \frac{\partial E}{\partial \theta_i} - J_s V_i \sin\theta_i \frac{\partial E}{\partial \phi_i} \\ -\frac{\partial E}{\partial \theta_i} + \frac{\alpha}{\sin\theta_i}\frac{\partial E}{\partial \phi_i} \end{pmatrix}. \end{aligned} \tag{7}$$

Let us denote $\eta_{2i-1} = p_i$ and $\eta_{2i} = q_i$. We can write the equation of motion in the form,

$$\frac{\partial \eta_{2i-1}}{\partial t} = \frac{\partial p_i}{\partial t} =: f_{2i-1}(\eta_1, \ldots, \eta_{2N}), \tag{8}$$

$$\frac{\partial \eta_{2i}}{\partial t} = \frac{\partial q_i}{\partial t} ==: f_{2i}(\eta_1, \ldots, \eta_{2N}). \tag{9}$$

Transition state theory considers the linear dynamics around the saddle point. Linearizing the right hand side around the saddle point, we obtain

$$\begin{pmatrix} \frac{\partial \eta_1}{\partial t} \\ \vdots \\ \frac{\partial \eta_{2N}}{\partial t} \end{pmatrix} \approx \begin{pmatrix} f_1 \\ \vdots \\ f_{2N} \end{pmatrix}\Bigg|_{sp} + \begin{pmatrix} \frac{\partial f_1}{\partial \eta_1} & \cdots & \frac{\partial f_1}{\partial \eta_{2N}} \\ \vdots & \ddots & \vdots \\ \frac{\partial f_{2N}}{\partial \eta_1} & \cdots & \frac{\partial f_{2N}}{\partial \eta_{2N}} \end{pmatrix}\Bigg|_{sp} \begin{pmatrix} \eta_1 - \eta_{sp,1} \\ \vdots \\ \eta_{2N} - \eta_{sp,2N} \end{pmatrix}. \tag{10}$$

The first derivatives of the energy with respect to the spin components at the saddle point are zero, thus, the first term on the right hand side is zero as well. The second term we define as H_{dyn}

$$H_{dyn} := \begin{pmatrix} \frac{\partial f_1}{\partial \eta_1} & \cdots & \frac{\partial f_1}{\partial \eta_{2N}} \\ \vdots & \ddots & \vdots \\ \frac{\partial f_{2N}}{\partial \eta_1} & \cdots & \frac{\partial f_{2N}}{\partial \eta_{2N}} \end{pmatrix}\Bigg|_{sp}. \tag{11}$$

The last term we define as vector $\nu_k = \eta_k - \eta_{sp,k}$. The time derivative of $\vec{\nu}$ equals the left hand side of Eq. (10). So Eq. (10) can be written as

$$\frac{\partial \vec{\nu}}{\partial t} \approx H_{dyn}\vec{\nu}. \tag{12}$$

This is a linear system of differential equations which has 2N eigenvalues λ_k with corresponding eigenvectors $\overrightarrow{\nu_k^0}$. The solutions are of the form

$$\overrightarrow{\nu_k} = \overrightarrow{\nu_k^0} e^{\lambda_k t}. \tag{13}$$

With the exception of one eigenvalue, all other eigenvalues of the matrix H_{dyn} at the saddle point are negative. This single positive eigenvalue is the λ_+ that we need for the calculation of the attempt frequency.

For the numerical calculation of H_{dyn}, the function $f = f_i$ has to be derived with respect to the coordinate $x = \eta_i$. This was calculated numerically using finite differences and a seven point stencil method.

$$f'(x) \approx \frac{-f(x-3h) + 9f(x-2h) - 45f(x-h) + 45f(x+h) - 9f(x+2h) + f(x+3h)}{60h}. \tag{14}$$

The step size used in the numerical results was $h = 0.005$.

B. Statistical factor Ω_0 from the Hessian matrix

The statistical factor Ω_0 relates the curvature of the total energy with respect to the canonical variables at the saddle point and at the minimum. The curvature is obtained by calculating the second derivative of the energy,

$$\begin{aligned} H :&= \begin{pmatrix} \frac{\partial h_1}{\partial \eta_1} & \cdots & \frac{\partial h_1}{\partial \eta_{2N-2}} \\ \vdots & \ddots & \vdots \\ \frac{\partial h_{2N-2}}{\partial \eta_1} & \cdots & \frac{\partial h_{2N-2}}{\partial \eta_{2N-2}} \end{pmatrix} \\ &= \begin{pmatrix} \frac{\partial^2 E}{\partial \eta_1 \partial \eta_1} & \cdots & \frac{\partial^2 E}{\partial \eta_{2N-2} \partial \eta_1} \\ \vdots & \ddots & \vdots \\ \frac{\partial^2 E}{\partial \eta_1 \partial \eta_{2N-2}} & \cdots & \frac{\partial^2 E}{\partial \eta_{2N-2} \partial \eta_{2N-2}} \end{pmatrix}. \end{aligned} \tag{15}$$

Ω_0 is the square root of the ratios of the determinants of the Hessian matrices at the minimum and the saddle point

$$\Omega_0 = \sqrt{\frac{\det H_{min}}{|\det H_{sp}|}}. \tag{16}$$

It is important to note that the theory of transitions as developed by Langer is only valid for canonical variables. Suppose that instead of the canonical variables (p_i, q_i), the polar angles (θ_i, ϕ_i) are used to describe the system (see, e.g., Ref. 18) and its derivatives $\frac{\partial^2 E}{\partial \theta_i \partial \phi_i}$. Then, the obtained f_0 is correct only if the magnetic state at the minimum and the saddle point fulfills $\theta_i = \pi/2$ for all spins. This prerequisite is, for example, fulfilled for a single domain particle having the easy axis pointing along the x-axis and an external field applied along the y-axis as in Ref. 18. The same argument applies for the calculation of λ_+.

For the numerical calculation of the derivative, the same finite difference scheme was used as described in Sec. II A.

C. Climbing image nudged elastic band method

The calculation of the statistical prefactor Ω_0 and the calculation of λ_+ require knowledge of the saddle point configuration. A very accurate calculation of the saddle point configuration is essential for the calculation of the attempt frequency. The nudged elastic band method was used in order to calculate the saddle point configuration.[8,21] It was found that the accuracy of the nudged elastic band method is not sufficiently high in order to calculate reliably the attempt frequency. In order to improve the accuracy of the saddle point determination, a climbing image elastic band method was implemented.[12]

III. VALIDATION OF THE METHOD

A. Small magnetic cube

In order to test the numerical calculation of the attempt frequency, we compared the analytically obtained attempt frequency for a single domain particle with uniaxial anisotropy to the numerically obtained one. For the numerical model, the following parameters were used: damping constant $\alpha = 1$, anisotropy constant $K_1 = 1.0\, MJ/m^3$, magnetic saturation polarization $J_s = 0.5T$, and exchange constant

$A = 10\ pJ/m$. The model size is $0.6 \times 0.6 \times 0.6\,\mathrm{nm}^3$. 12 finite elements were used to discretize the cube. The easy axis of the cube was assumed to be parallel to the x-axis. The external field was applied parallel to the y-axis. Results were compared with those obtained using the analytically derived expression for the attempt frequency given in Ref. 18.

In Fig. 1(b), two magnetization states of the homogeneous cube are shown: on the left, the initial state is depicted, with magnetization pointing close to the easy axis. On the right, the magnetization is shown at the saddle point of the energy, where the magnetization is perpendicular to the easy axis. The magnetization vectors of all nodes are shown. Due to the small structure size, all spin vectors are almost perfectly parallel to each other, indicating that we should expect a good agreement with the analytic result.

In order to compare the numerical results directly with the analytical results, the attempt frequency is plotted as a function of the external field strength as shown in Fig. 1(a). The simulations agree very well with the analytical solution. It should be noted that both the analytical solution and the numerical simulation are not valid for zero external field, since the expressions for field lowered symmetry are used. As a consequence, the spike-like increase at zero external field is an artifact and has no physical meaning.

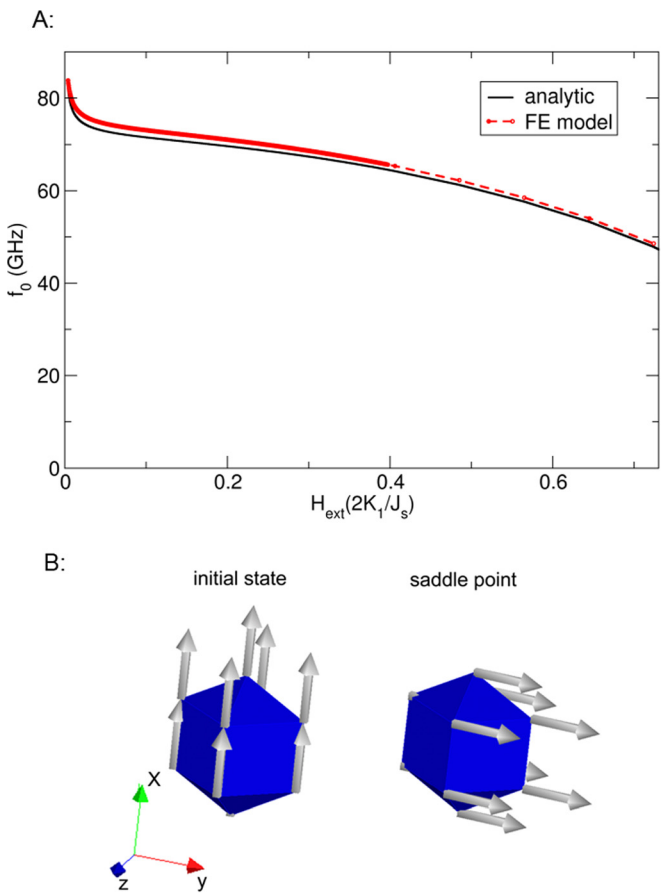

FIG. 1. (a) The numerically calculated attempt frequency of a small magnetic particle is compared with the analytical result as a function of the external applied field (H field applied along y-axis, easy axis parallel to x-axis). (b) The magnetic state at the minimum (left) and at the saddle point (right) are shown.

B. Elongated particle

As a second example, we calculate the attempt frequency of an elongated particle. The simulated geometry of the elongated grain is: length 25 nm, width 1.6×1.6 nm. This shape is similar to the magnetic grains used as the recording media in modern hard disks, only slimmer (die lateral dimension of a grain of a hard disc is about 6×6 nm). According to the analytical theory of Ref. 16, the cross section area does not influence the attempt frequency. Hence, in order to save computational time, we model the grain of a recording media with a smaller cross section, but we can expect that the results can be used for realistic grains.

The following parameters were used for the graded media grain example: damping constant $\alpha = 0.2$, anisotropy constant increasing quadratically from zero to $K_1 = 3.6\ \mathrm{MJ/m}^3$, magnetic saturation polarization $J_s = 0.5\mathrm{T}$, and exchange constant $A = 10\ \mathrm{pJ/m}$. The material parameters are the same as in Ref. 22.

Fig. 2 shows the simulated grain with quadratically increasing K_1. The directions of the easy-axis and the applied perpendicular external magnetic field are shown. The magnetic state at the minimum of the energy is shown on the left side of the figure, and the saddle point is shown on the right side.

As in Sec. III A, the attempt frequency was calculated as a function of a perpendicular applied field. In order to verify reliability, the simulations were repeated with different finite element meshes.

Fig. 3 shows the attempt frequency of four different finite element meshes, with different numbers of volume elements. As can be seen, the results of the attempt frequency do not converge to a single value as the finite element mesh size is decreased. Furthermore, the obtained value of the attempt frequency is one order of magnitude larger than the value reported in Ref. 22. The reason for these discrepancies is discussed in Sec. IV.

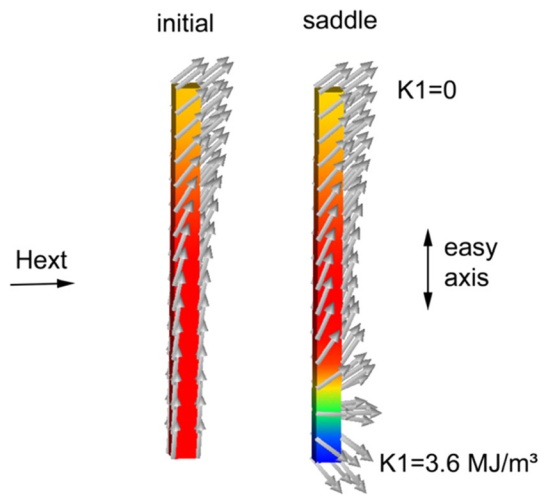

FIG. 2. Model of the graded media grain which is soft magnetic at the top and hard magnetic at the bottom. (left) energy minimum state (right) saddle point configuration.

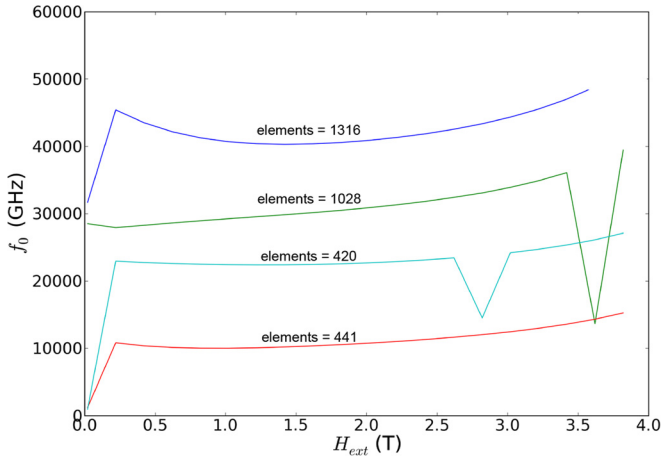

FIG. 3. The attempt frequency as a function of the external field strength is shown for a graded media grain. The external field is applied perpendicular to the easy axis. The results are shown as a function of the number of finite elements.

IV. IMPROVED METHOD USING ANALYTICAL FITS

The reason for the numerical errors of the attempt frequency can be found in the calculation of Ω_0, which consists of (the square root of) a ratio of determinants as given by Eq. (16). The calculation of the determinant of the symmetric matrix H equals the product of all its eigenvalues $\lambda_1, \ldots, \lambda_{2N}$, where N is the number of finite element node points.

Hence, we can write Ω_0 in the form

$$\Omega_0 = \sqrt{\frac{\prod \lambda_{min_i}}{|\prod \lambda_{sp_i}|}} = \sqrt{\left|\frac{\prod \lambda_{min_i}}{\prod \lambda_{sp_i}}\right|}.$$

All eigenvalues of H_{min} at the minimum are positive. At the saddle point, there is only one negative eigenvalue. The number of eigenvalues increases with increasing number of finite elements. Hence, small numerical errors in the calculation of the eigenvalues multiply together to form a considerable total error.

Fig. 4 shows the ratio of the eigenvalues. The x-axis represents the index i of the eigenvalues, and the y-axis represents the natural logarithm of the ratios of eigenvalues, $\lambda_{min,i}/\lambda_{sp,i}$. In Fig. 4, the eigenvalues are sorted according to modulus, where the eigenvalue with the index $i = 1$ has the smallest modulus, and $i = 2N$ is the eigenvalue with the largest modulus. As shown in Fig. 4, only ratios of eigenvalues with small i are not close to or equal to 1. All the ratios of the eigenvalue with $i \gg 100$ are very close to one, which results in $\ln(\lambda_{min,i}/\lambda_{sp,i}) \approx 0$ for $i \gg 100$.

The numerical evidence in Fig. 4 illustrates the insensitivity of the saddle point to the majority of eigenmodes and the thermal significance of modes with the smallest eigenvalues. As noted in Ref. 15, a domain wall pinned at an interface supports a broad range of travelling spin waves that are essentially unperturbed by the wall structure, and a set of modes localized to the domain wall. The modes localized to the wall have the smallest eigenvalues and represent the most relevant fluctuations for thermal depinning of the wall.

Braun has shown that for elongated particles, the logarithm of the ratio of eigenvalues scales with $\frac{i}{1+i^2}$ (see formula (4.12) of Ref. 1).

In order to reduce the numerical error which is introduced by the higher order eigenfrequency, we fit the values of $\ln(\lambda_{min,i}/\lambda_{sp,i})$ to the following function:

$$f(i) = a \cdot \left(\frac{i}{1+i^2}\right)^b, \tag{17}$$

where a and b are parameters determined by a mean square fit to the numerical data for $5 < i < 60$. In Fig. 5, the black line represents the ratios of eigenvalues, calculated by the numerical simulation, and the red line is the fitted function, which values of parameters a and b are given in the inset. The calculation of Ω_0 is done by calculating $\Omega_0 = \sqrt{\left|\prod_{i=0}^{c} \frac{\lambda_{min_i}}{\lambda_{sp_i}} \cdot \prod_{i=c+1}^{N} e^{fit(i)}\right|}$. We found for a wide range

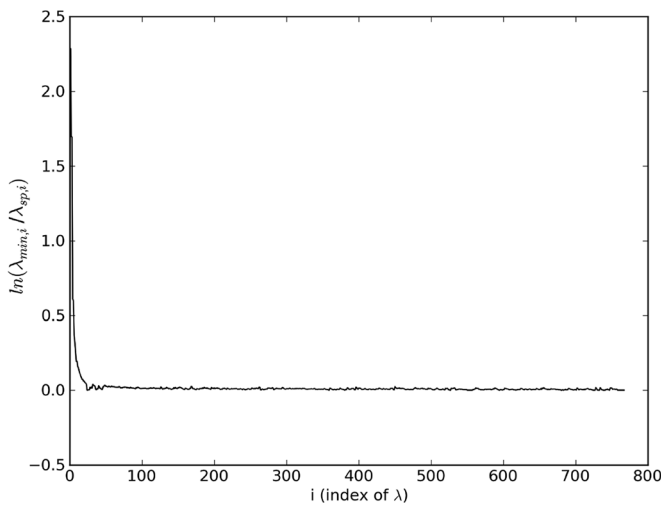

FIG. 4. Logarithmic ratios of eigenvalues as a function of the eigenvalue index i. (number of finite elements = 1316, H_{ext} is 0.02 T.)

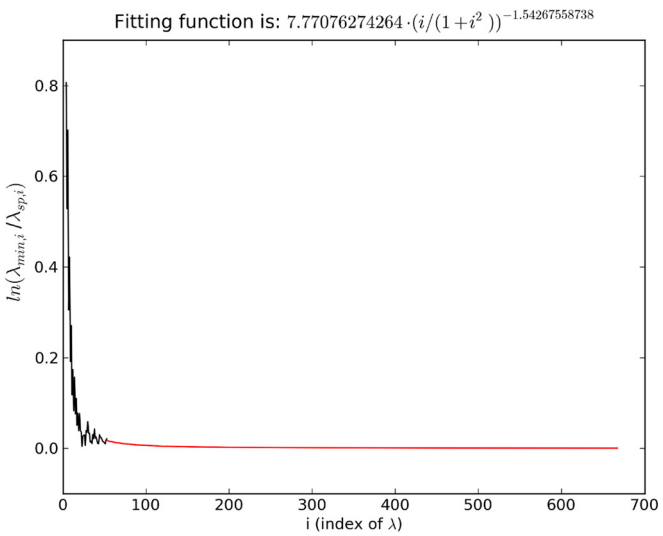

FIG. 5. Contributions to calculation of Ω_0: up to index 50, the original data are taken (black line), and from index 50 onwards, the values of the fitting function are used (red line).

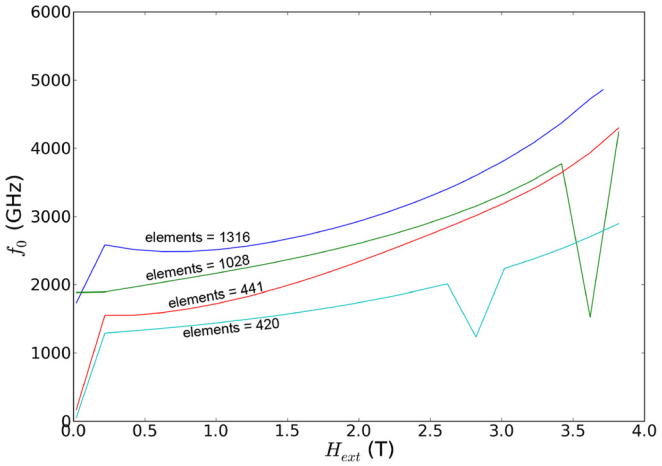

FIG. 6. Same as Fig. 3 except that a fitting function from eigenvalue index 30 onwards is used for the calculation of Ω_0.

of c ($10 < c < 100$) that the value of Ω_0 is not significantly influenced by the actual chosen value of the parameter c.

The calculation of the attempt frequency of the graded media grain is repeated with the improved method using the fit function. Fig. 6 shows that the mesh dependency of the results is decreased by this method. If the value of the attempt frequency is extrapolated for an external field approaching zero we can estimate the attempt frequency to be in the order of $f_0 \sim 1850\text{GHz} \pm 650\text{GHz}$. Comparing this estimate of the attempt frequency with the estimate of the attempt frequency obtained by Langevin dynamic simulations (in Ref. 22, for the same system, a value of $f_0 \sim 1638\text{GHz} \pm 46\text{GHz}$ is estimated), despite the various assumptions, which are used in both methods, a considerable good agreement can be found.

From an application point of view, it is interesting to compare the attempt frequency of a grain with graded anisotropy to the attempt frequency of grain for which anisotropy is uniform throughout. Fig. 7 shows the attempt frequency of a single phase grain, where all the material parameters are the same as for the graded media grain of Fig. 6 except that the anisotropy is a constant $K_1 \sim 3.6$ MJ/m^3. This value

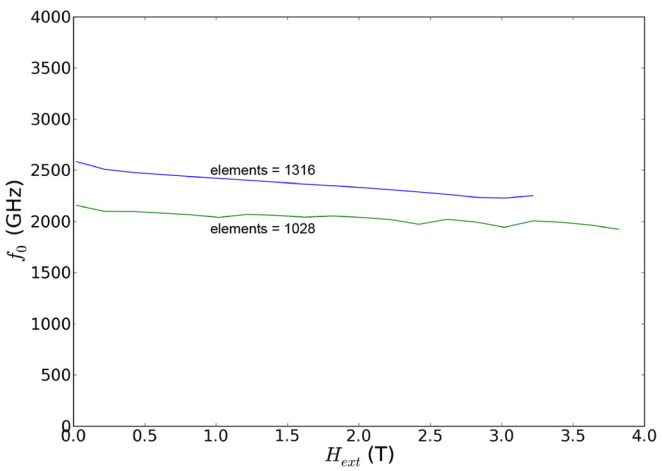

FIG. 7. Attempt frequency of a single phase media calculated for two different mesh sizes (for the calculation of Ω_0 a fitting function from eigenvalue index 30 onwards is used).

equals the maximum anisotropy constant of the graded media grain of the previous results.

V. RESULTS AND DISCUSSION

A numerical implementation of the transition state theory was described with application to two example problems: reversal of a single phase and graded media magnetic grains. The implementation makes use of the micromagnetic package FEMME. This method allows for the calculation of the long term thermal stability of magnetic nanostructures without any free parameters. The input parameters of the model are the exchange constant, the anisotropy constant, the spontaneous saturation magnetization, the damping constant, and the geometry of the magnet. The advantage of the presented method over Langevin-dynamic simulation is that the thermal stability of large magnetic nanostructures can be calculated. Furthermore, Langevin-dynamic simulations are restricted to time scales of several nano-seconds due to computational effort.

In previous work, it was shown that so called exchange spring media exhibit superior writeability as compared to single phase media, without lowering the energy barrier.[20] The energy barrier was assumed to determine the thermal stability. In this paper, we show the exact relation of the energy barrier and the thermal stability by calculating the attempt frequency. In the present paper, we show that the attempt frequency and energy barrier are comparable for a single phase media and a graded media grain with single phase grain anisotropy is the same as the maximum anisotropy in the graded media grain. Hence, it was shown that these two media types indeed have very similar thermal stabilities, but the coercive field for the graded media grain is about a factor of seven smaller than the single phase grain.

ACKNOWLEDGMENTS

The financial support of the FWF Project Nos. P20306-N16 and SFB ViCoM (F4112-N13) is acknowledged.

[1]H. B. Braun, "Statistical mechanics of nonuniform magnetization reversal," Phys. Rev. B **50**(22),16501 (1994).
[2]W. F. Brown, "Thermal fluctuations of fine ferromagnetic particles," IEEE Trans. Magn. **15**(5), 1196–1208 (1979).
[3]W. F. Brown, "Thermal fluctuations of a single-domain particle," Phys. Rev. **130**(5), 1677–1686 (1963).
[4]W. T. Coffey, D. S. F. Crothers, J. L. Dormann, L. J. Geoghegan, and E. C. Kennedy, "Effect of an oblique magnetic field on the superparamagnetic relaxation time. II. Influence of the gyromagnetic term," Phys. Rev. B **58**(6), 3249–3266 (1998).
[5]W. T. Coffey, D. S. F. Crothers, J. L. Dormann, Yu. P. Kalmykov, E. C. Kennedy, and W. Wernsdorfer, "Thermally activated relaxation time of a single domain ferromagnetic particle subjected to a uniform field at an oblique angle to the easy axis: Comparison with experimental observations," Phys. Rev. Lett. **80**(25), 5655–5658 (1998).
[6]W. T. Coffey, D. A. Garanin, and D. J. McCarthy, *Crossover Formulas in the Kramers Theory of Thermally Activated Escape Rates—Application to Spin Systems*, Advances in Chemical Physics, Vol. 117 (Wiley, 2001).
[7]P. M. Déjardin, D. S. F. Crothers, W. T. Coffey, and D. J. McCarthy, "Interpolation formula between very low and intermediate-to-high damping kramers escape rates for single-domain ferromagnetic particles," Phys. Rev. E **63**(2 pt I), 0211021 (2001).
[8]R. Dittrich, T. Schrefl, D. Suess, W. Scholz, H. Forster, and J. Fidler, "A path method for finding energy barriers and minimum energy paths in

complex micromagnetic systems," J. Magn. Magn. Mater. **250**, L12–L19 (2002).
[9]D. A. Garanin, E. C. Kennedy, D. S. F. Crothers, and W. T. Coffey, "Thermally activated escape rates of uniaxial spin systems with transverse field: Uniaxial crossovers," Phys. Rev. E **60**(6), 6499 (1999).
[10]J. L. García-Palacios and D. A. Garanin, "Nonlinear response of superparamagnets with finite damping: An analytical approach," Phys. Rev. B **70**(6), 064415 (2004).
[11]C. W Gardiner, *Handbook of Stochastic Methods* (Springer, Berlin, 1985).
[12]G. Henkelman, B. P. Uberuaga, and H. Jonsson, "A climbing image nudged elastic band method for finding saddle points and minimum energy paths," J. Chem. Phys. **113**(22), 9901 (2000).
[13]H. A. Kramers, "Brownian motion in a field of force and the diffusion model of chemical reactions," Physica **7**(4), 284–304 (1940).
[14]J. S. Langer and L. A. Turski, "Hydrodynamic model of the condensation of a vapor near its critical point," Phys. Rev. A **8**(6), 3230–3243 (1973).
[15]K. L. Livesey, D. C. Crew, and R. L. Stamps, "Spin wave valve in an exchange spring bilayer," Phys. Rev. B **73**(18), 184432 (2006).
[16]P. N. Loxley and R. L. Stamps, "Theory for nucleation at an interface and magnetization reversal of a two-layer nanowire," Phys. Rev. B **73**(2), 1–14 (2006).
[17]E. Magyari, H. Thomas, R. Weber, C. Kaufman, and G. Müller, "Integrable and nonintegrable classical spin clusters—integrability criteria and analytic structure of invariants," Z. Phy. B: Condens. Matter **65**(3), 363–374 (1987).
[18]J. Schratzberger, J. Lee, M. Fuger, J. Fidler, G. Fiedler, T. Schrefl, and D. Suess, "Validation of the transition state theory with langevin-dynamics simulations," J. Appl. Phys. **108**(3), 033915 (2010).
[19]D. A. Smith and F. A. De Rozario, "A classical theory of superparamagnetic relaxation," J. Magn. Magn. Mater. **3**(3), 219–233 (1976).
[20]D. Suess, "Multilayer exchange spring media for magnetic recording," Appl. Phys. Lett. **89**, 113105 (2006).
[21]D. Suess, S. Eder, J. Lee, R. Dittrich, J. Fidler, J. W. Harrell, T. Schrefl, G. Hrkac, M. Schabes, N. Supper, and A. Berger, "Reliability of sharrocks equation for exchange spring bilayers," Phys. Rev. B **75**(17), 174430 (2007).
[22]D. Suess, J. Fidler, G. Zimanyi, T. Schrefl, and P. Visscher, "Thermal stability of graded exchange spring media under the influence of external fields," Appl. Phys. Lett. **92**, 173111 (2008).
[23]D. Suess, V. Tsiantos, T. Schrefl, J. Fidler, W. Scholz, H. Forster, R. Dittrich, and J. J. Miles, "Time resolved micromagnetics using a preconditioned time integration method," J. Magn. Magn. Mater. **248**(2), 298–311 (2002).